energy&fuels

Article

pubs.acs.org/EF

Reaction Dynamics of Rocket Propellant with Magnesium Oxide Nanoparticles

Michael N. Bello,[†] Michelle L. Pantoya,[*,†] Keerti Kappagantula,[‡] William S. Wang,[§] Siva A. Vanapalli,[§] David J. Irvin,[∥] and Leslie M. Wood[∥]

[†]Department of Mechanical Engineering, and [§]Department of Chemical Engineering, Texas Tech University, Lubbock, Texas 79409, United States

[‡]Department of Mechanical Engineering, Ohio University, Athens, Ohio 45701, United States

[∥]Systems and Materials Research Corporation, Austin, Texas 78756, United States

Supporting Information

ABSTRACT: The combustion behavior of rocket propellant grade 2 (RP-2) was investigated as a function of magnesium oxide (MgO) nanoparticles (i.e., 20 nm diameter) added at varied concentrations. The MgO nanoparticles were surface-treated with a long-chain carboxylic acid to aid their dispersion in RP-2. The fuel droplet regression rate, surface tension, and heat of combustion of RP-2 with MgO nanoparticle additives were measured to characterize combustion behavior. Heat of combustion and surface tension measurements varied negligibly among all samples indicating that calorific output and surface tension are not controlling parameters influencing fuel combustion behavior. However, fuel droplet regression rates were considerably increased by adding 0.5 wt % MgO from 0.225 to 66.16 mm/s, which is an improvement by 2 orders of magnitude. Further analysis showed that MgO particles enhance diffusive heat transfer, which promotes nucleation and disruptive burning throughout the three stages of regression, heating/evaporation (stage 1), combustion of RP-2 (stage 2), and combustion of carboxylic acid dispersant (stage 3), and, thus, lead to improved fuel droplet combustion.

INTRODUCTION

Propellants with improved performance are a compelling need for next-generation propulsion systems. The regression rate is an indicator of propellant performance and defines the rate that a liquid droplet surface recedes over the course of its evaporation and combustion in the presence of an ignition source.[1] An approach for improving the regression rate of rocket propellants is to include particulate additives that affect evaporation and burning behavior. Thus, understanding how solid particles influence combustion behavior is key for optimizing the performance of next-generation liquid fuels.

Particle additives introduced into liquid fuels can agglomerate and, thus, work best when they are well-dispersed in the liquid. Typically, a dispersant is added to the liquid fuel, which by itself does not significantly alter the regression rate or burn rate constant but improves the dispersion quality of the particles.[2,3] The particle size is also important, and nanoparticles optimize regression far more than their micrometer-scale counterparts.[4] Initial experimental work studying solid particle additives in liquid fuels focused on high concentrations of micrometer-size particles added to liquid propellant systems, but there were significant problems associated with them. Micrometer additives often agglomerate during evaporation and combustion of the fuel droplets, resulting in slow droplet regression rates and decreased combustion efficiency.[5] Later research focused on nanoparticle additives with a higher surface area to volume ratio compared to micrometer particles, facilitating more direct contact between the particles and liquid, leading to more complete combustion and higher combustion efficiency.[6,7] Gan and Qiao[4] compared the burning characteristics of ethanol- and *n*-decane-based fuel droplets with nano- and micrometer-sized aluminum (Al) particles in the presence of a dispersant. Their results reveal that, for the same particle loading and dispersant concentration, the disruption of the fuel droplet with nanoparticle suspension occurred earlier and promoted faster droplet regression compared to micrometer particles. Nanoparticles also demonstrate enhancements in convective heat transfer at earlier times, and they showed that particle agglomeration played an overall negative role in the burning characteristics of fuel droplets.[4] Gan and Qiao[8] also measured the transmission spectrum of fluids with nanoparticle additives and demonstrated that the evaporation rates during combustion of ethanol-based fuels containing multi-walled carbon nanotubes (CNTs), Al, and carbon nanoparticles (CNPs) are higher (25.6% CNT, 18.7% Al, and 5.7% CNP, respectively) than the evaporation rate of pure ethanol. The optical properties, such as transmission spectrum and extinction coefficient, of the nanofluid correlated with energy build up and regression behavior.[8] All of these studies suggest that particulate additives can enhance heat transfer and promote evaporation and burning of the liquid fuel, whereas particle agglomeration can have a negative effect counterbalancing the advantages of enhanced heat transfer. In fact, nanoparticles are the only size particle additives studied in the most recent literature such that the term nanofluid droplet combustion has been adopted to describe liquid fuels with nanoparticle additives.

Received: April 24, 2015
Revised: August 4, 2015

ACS Publications © XXXX American Chemical Society

DOI: 10.1021/acs.energyfuels.5b00905
Energy Fuels XXXX, XXX, XXX−XXX

Most studies attribute improved nanofluid droplet combustion to enhanced heat transfer. Researchers have studied thermal conductivity, natural and weak forced convection, and radiative properties associated with these liquid−solid phase mixtures.[4,8,9] There are limited studies investigating the influence of surface tension[10] and calorific output such that experimental investigations are needed to provide an empirical perspective on fundamental modeling of multiphase combustion.

Tyagi et al.[11] studied droplet ignition of diesel with and without Al and aluminum oxide (Al_2O_3) nanoparticles. They examined droplets atop a hot plate over a range of temperatures from 688 to 768 °C. They observed that, for even small additive concentrations (0.1−0.5 vol %), the ignition time of the nanofluid was significantly lower than that of pure diesel fuel and attributed this difference to improved heat transfer properties promoted by the nanoparticles. Allen et al.[12] also studied Al nanoparticles suspended in JP-8 and observed that, by adding 2 wt % Al, the ignition delay of the fuels reduced by 50%. Van Devener and Anderson experimented with cerium oxide (CeO_2) and iron oxide (Fe_2O_3) particles suspended in JP-10 because these materials provide naturally catalytic surfaces that were proposed to accelerate ignition and combustion of the hydrocarbons in the fuel.[13] They found that the catalysts initiates the JP-10 breakdown process, generating CO, CO_2, H_2O, and H_2CO, promoting efficient combustion.[13]

Javed et al. reported a series of investigations that examine the impact of Al particles with oleic acid (OA) used as the surface coating to aid dispersion of the particles on different liquid fuels, such as kerosene and heptane.[2,3,14] In all of these studies, the droplet is maintained in a temperature-controlled environment ranging from ambient to as high as 800 °C such that evaporation can be observed. They identified a three-stage evaporation process corresponding to a finite heating period (stage 1), evaporation of the highly volatile liquid fuel (stage 2), followed by evaporation of the low-volatility dispersant (stage 3) and observed disruptive evaporation attributed to bubble formation and microexplosions induced by nucleation sites, resulting from the nanoparticles.

The addition of solid particle additives to liquid propellants affect heat transfer and combustion by controlling parameters, including the concentration, particle size, and dispersion quality. In addition, surface tension and altered stoichiometry introduced by the solid additives also influence evaporation and combustion. The purpose of this study is to experimentally examine the reaction dynamics of a rocket propellant, RP-2, containing magnesium oxide (MgO) nanoparticles dispersed using OA, a long-chain carboxylic acid dispersant. These nanofluids are characterized for their combustion performance by measuring droplet regression rates and burn rate constants upon thermal ignition, measuring heat of combustion using a bomb calorimeter, and examining surface tension. It is noted that preliminary tests show OA dispersant alone has a negligible effect on the regression rate and burn rate constant but that its primary function is dispersion of the solid particles (also observed by Javed et al.,[2,3]). Particles of MgO were selected for this study because preliminary research examining dispersion qualities of nanoparticles showed that MgO produced excellent dispersion characteristics relative to other nanoparticle additives.[31] Also, thermal and physical properties for MgO are listed in Table 1 alongside additives, such as Al and CNT.[15−19]

Table 1. Properties of Some Propellant Additives

thermal property	MgO	CNT	Al
molar mass (g/mol)	40.3	12.0	27.0
thermal conductivity (W m^{-1} K^{-1})	42	3000	237
heat capacity (J kg^{-1} K^{-1})	877	450	1000
density (kg/m^3)	3580	1740	2700
thermal diffusivity (×10^{-5}, m^2/s)	1.338	383	8.778
emissivity	0.55	0.98	0.20

EXPERIMENTAL SECTION

The base propellant used for this study is rocket propellant grade 2 (RP-2), supplied by the U.S. Air Force, Eglin Air Force Base, and used as received. The MgO solid particle additive is introduced in varying concentrations and has a 20 nm average diameter from Nanostructured and Amorphous Materials, Inc. of Houston, TX, detailed in Table 2. The size distribution is measured by Brownian motion using a Nanosight LM10 instrument. A dispersant, OA (Sigma-Aldrich) was also added to the propellant to facilitate MgO suspension and avoid particle agglomeration. The appropriate amount of MgO was placed in 20 mL of RP-2 and sonicated using a Qsonica Q700 (35% power) sonicator equipped with a tapered microtip for 10 min. The additive to dispersant ratio was consistently maintained at 1:10. The appropriate amount of OA was then added, and the sample was again sonicated for 10 min. During sonication, the vial was placed in a water bath to prevent excessive heating. The horn was placed in the suspension, and sonication was performed at an amplitude of 35%.

Table 2. Compositions Examined in the Current Study

RP-2
RP-2 + 0.05 wt % MgO
RP-2 + 0.25 wt % MgO
RP-2 + 0.50 wt % MgO
RP-2 + 0.75 wt % MgO
RP-2 + 1 wt % MgO

It is noted that preliminary tests using RP-2 with varied dispersant concentrations and without the nanoparticle additive indicated no significant differences in the RP-2 regression rate, droplet surface tension, or calorific output compared to RP-2 alone. The MgO suspensions of less than 0.5 wt % were found to be stable for over 30 days without a change in aggregate size or precipitation. The higher concentration samples showed signs of precipitation, but the aggregate sizes did not change.

Regression Rate Measurements. Figure 1 shows a schematic of the experimental setup originally developed by Datta et al.[20] and adopted here to analyze droplet combustion. A 1 mm diameter quartz fiber with a circular cross-section acted as the support for fuel droplet suspension. It is noted that Law et al.[32] showed that interference from distortion and heat loss can be considered to be unimportant during much of the droplet lifetime for fiber diameters less than 100 μm, such that the 1 mm diameter fiber used here may introduce a source of error from interference by enhancing the gasification rate. Heat transfer through the fiber is more efficient than that through the gas medium between the flame and the droplet surface. However, the same fibers were used for all samples investigated to ensure consistency, such that the trends in behavior among dispersions should be repeatable. Droplets were introduced onto the quartz fiber using a syringe. The shape of the suspended droplet on the support fiber was naturally distorted from spherical to ellipsoidal, owing to gravity effects. Consistent with other research,[21] the maximum diameter was measured as a function of time assuming that gravitational distortion was the same for all of the droplets. In each test, care was taken to ensure all droplets had an initial average diameter of 2.0 mm. All experiments were performed in triplicate to establish repeatability.

DOI: 10.1021/acs.energyfuels.5b00905
Energy Fuels XXXX, XXX, XXX−XXX

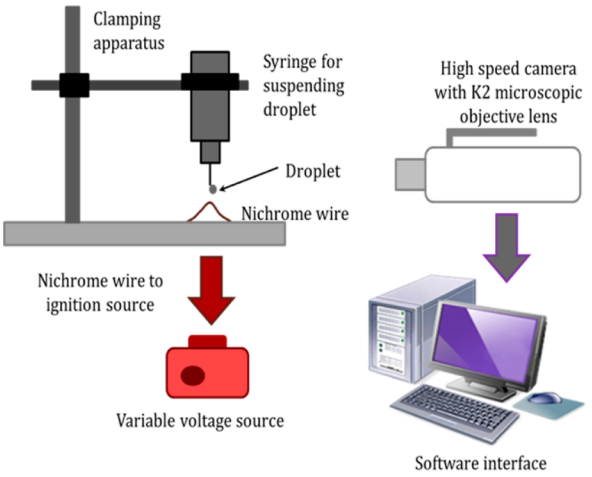

Figure 1. Schematic of the experimental apparatus for measuring the regression rate, including droplet syringe, voltage source for ignition, high-speed camera, and software interface.

A 0.508 mm diameter nichrome (Omega Engineering, 80% nickel and 20% chromium) wire was bent and attached to an acrylic plate. The acrylic plate was then positioned underneath the droplet and connected to a voltage source to resistively heat and ignite the fuel droplets. A consistent 3 V alternating current (AC) current was supplied to the nichrome wire, and all samples achieved ignition.

A Phantom IV (Vision Research, Wayne, NJ) high-speed camera was used to image droplet regression rates. A K2 long-distance microscope lens (Infinity Photo-Optical Company, Boulder, CO) was attached to the high-speed camera for higher magnification. A fiber optic light source (Cole Parmer Illuminator, 41720 series) was used to increase the contrast between the droplets and background for improved visualization. High-speed images of droplet combustion were analyzed using the Vision Research software interface to determine the droplet surface regression rate. From the captured images, the Vision Research software works on a contrast difference bases (bright edges versus dark edges) to identify the edges of the droplet. The software gives the droplet edge position (in pixels) over time. This position in pixels is converted to diameter using a scaling factor and reference value previously defined by the operator and input into the camera. These diameters are measured alongside the time scale between frames, to calculate the regression rate.

Heat of Combustion Measurements. Samples of RP-2 with and without MgO nanoparticles, weighing 500 mg, were placed in a metal crucible in the Parr 1108 oxygen combustion bomb (Parr Instrument Company, Moline, IL). The bomb was sealed, filled with 30 atm of pure oxygen, connected to the Parr 2901 ignition unit, and placed in a Parr 1341 oxygen bomb calorimeter, comprising 2 kg of distilled water in a bath. The top of the calorimeter houses a stirring device driven by a small motor, which circulated the water continuously. A thermocouple inserted in the water bath measured temperature for 60 min of experimentation. The first 10 min allowed the water bath to attain thermal equilibrium, and then the sample in the calorimeter was ignited. The thermocouple recorded about 35 000 temperature measurements as a function of time during combustion. These values were used to calculate the heat of combustion of the samples according to the ASTM standard.[22]

Surface Tension Measurements. Surface tension was obtained by imaging pendant droplets of the various samples and using the selected plane method.[23,24] Figure 2A is a schematic diagram of the experimental setup for measuring surface tension. Syringes with 1 mL capacity were filled with the RP-2 nanofluid samples, fitted with 18-gauge blunt needle tips, and secured vertically, so that droplets could be produced at and suspended from the needle tip. A container was placed beneath the syringe for collecting droplets. For each sample, individual droplets were produced and remained suspended and static for a few moments before photographing from the side. Stauffer et al.

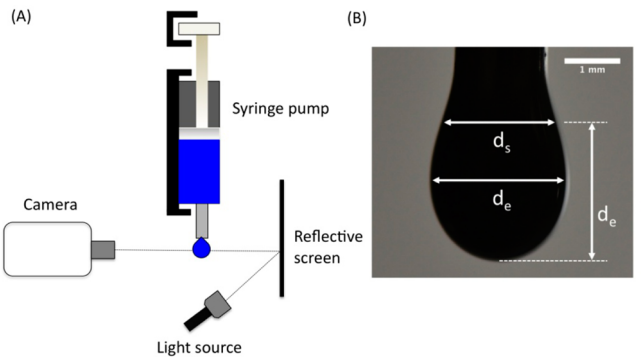

Figure 2. (A) Schematic of the experimental setup used to measure the surface tension of the nanoparticle-loaded liquid fuel and (B) image of a pendant droplet illustrating the equatorial and selected-plane diameters.

showed that measurement error decreased as the droplet shape became more oblong (i.e., larger shape factors and larger droplets);[24] therefore, droplets as large as possible were produced before imaging. Profile images of the droplets when they were thus suspended were taken with a Nikon D5100 digital SLR camera with an adjustable-zoom lens, and droplet edge contrast was improved using back illumination through a vertical glass plate covered with white paper. The equatorial diameter (d_e) and selected-plane diameter (d_s) shown in Figure 2B, were measured using ImageJ (version 1.48) image analysis software.

The interfacial tension (γ) between two fluids was obtained from the two diameter measurements d_e and d_s using eqs 1−3[24,25]

$$\gamma = \frac{(\rho_1 - \rho_2) g d_e^{\,2}}{H} \tag{1}$$

$$S = \frac{d_s}{d_e} \tag{2}$$

$$\frac{1}{H} = 0.3161 S^{-2.6040} \tag{3}$$

where the variables ρ_1 and ρ_2 are the densities of RP-2 and air, respectively, g is the acceleration due to gravity, H is an empirically determined function of the shape factor, and S is the shape factor of the suspended fuel droplets. Equation 3 was obtained through a power-law fit to the data relating shape function (H) to shape factor (S) presented by Tucker and Stauffer.[23,24] The above analysis was typically conducted on five RP-2 nanofluid samples, and the standard deviation for surface tension measurements was less than 4%.

RESULTS

Figure 3 shows the normalized droplet diameter as a function of time to illustrate the various stages of regression. Droplet diameter, D, is normalized against the initial droplet diameter, D_o. Figure 3A is for pure RP-2 and demonstrates that droplet regression occurred nonlinearly in two stages with higher and lower combustion rate constants and a negligible initial heating period. This behavior may result from the fiber affecting heating as well as the multicomponent nature of the droplet. Figure 3B shows RP-2 with 0.05 wt % MgO demonstrating three-stage regression (i.e., stages 1, 2, and 3). The stages are distinguished by inflection points on the curve through which dashed lines are drawn: stage 1 is a negligible initial heating period when the temperature of the droplet increases; stage 2 is a primary combustion period when the droplet burns, and stage 3 is the secondary combustion period when the dispersant burns. Figure 3B is representative of the three stages observed for all samples with MgO additives. Additional graphs of RP-2 with

DOI: 10.1021/acs.energyfuels.5b00905
Energy Fuels XXXX, XXX, XXX−XXX

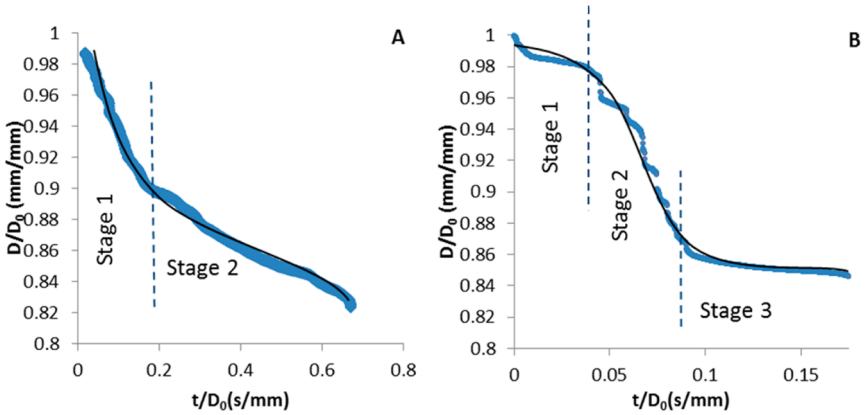

Figure 3. Stages of regression for (A) RP-2 and (B) RP-2 with 0.05 wt % MgO. Further data for other MgO concentrations are shown in Figure S1 of the Supporting Information.

varying concentrations of MgO (i.e., 0.25, 0.50, 0.75, and 1.0 wt %) are shown in Figure S1 of the Supporting Information. Similar stages were observed by Javed et al.[2] for kerosene with Al nanoparticles and OA dispersant, but their droplets were maintained in a constant temperature-controlled environment ranging from ambient to 800 °C. It is noted that 0.5 wt % MgO shows a unique two-stage heating period (Figure S1B and S2D). This unique behavior not seen with other concentrations of MgO may be a consequence of the optimized dispersion quality coupled with 20 nm particle size that promotes improved diffusive heat transfer, as will be discussed further.

Still frame images of RP-2 droplets with and without MgO during stages 2 and 3 are shown in panels A and B of Figure 4. Figure 4A shows a RP-2 droplet without additive, and Figure 4B shows RP-2 with 0.25 wt % MgO.

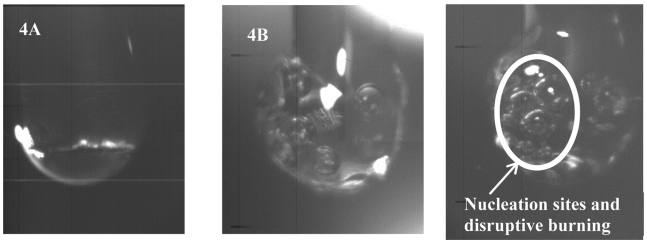

Figure 4. Still frame images of RP-2 with (A) no additives (stage 2), (B) 0.25 wt % MgO (stage 2), and (C) 0.25 wt % MgO showing nucleation sites circled and disruptive burning with an arrow and text.

Table 3 shows the time duration for each stage of regression as well as the burn rate constant K_b for the two combustion stages. The burn rate constant is calculated as the slope of the diameter squared versus time plot and given by eq 4,[25] with plots provided in Figure S2 of the Supporting Information. It is noted that, for pure RP-2 with a negligible heating period, stage 2 is represented in Table 3 with a higher combustion rate constant.

$$K_b = \frac{d(D^2)}{dt} \quad (4)$$

The droplet regression rate in stage 2, heat of combustion, and surface tension results are shown in Table 4. As a baseline for comparison, pure RP-2 droplets were examined and results show a 0.225 mm/s regression rate, 46.34 kJ/g heat of combustion, and 24.01 mN/m surface tension. The uncertainty associated with the measured regression rates is determined to be 0.28% based on repeatability studies of each data set (three tests for each composition), 4% for surface tension measurements based on repeatability of five tests for each composition, and 1% for heat of combustion based on repeatability of five tests for each sample.

Table 4 shows that MgO significantly affects the regression rate but not heat of combustion or droplet surface tension. A maximum regression rate of 66.16 mm/s is observed when 0.5 wt % MgO is added to the fuel; that is, about 2 orders of magnitude faster than the pure RP-2. The measured heats of combustion are all in the range of 44−46 kJ/g, with a higher solids concentration generally producing lower heats of combustion. Results also indicate that surface tension changes negligibly with the MgO concentration. These results are consistent with ref 10, which also showed a negligible impact of surface tension on regression.

Table 3. Time Durations (in Milliseconds) and Burn Rate Constants for Stages of Regression with Varying MgO Concentrations

MgO (wt %)	stage 1 duration (ms)	stage 2 duration (ms)	K_b stage 2 (mm^2/s)	stage 3 duration (ms)	K_b stage 3 (mm^2/s)
0	300	830	0.414	N/A	N/A
0.05	92	98	8.554	170	0.46
0.25	19	11	69.97	19	2.85
0.50	3	3	111.8	4	47.59
0.75	9	8	16.95	12	53.67
1	122	328	3.075	719	2.71

Table 4. Results for RP-2 with Varying MgO Concentrations[a]

MgO (wt %)	regression rate (mm/s)	heat of combustion (kJ/g)	surface tension (mN/m)
0	0.225	46.34	24.01
0.05	2.63	46.11	24.06
0.25	25.91	46.02	24.04
0.50	66.16	44.13	23.74
0.75	13.66	45.43	23.43
1	1.68	44.23	23.18

[a]Regression rate reported for stage 2 (i.e., combustion of RP-2).

DOI: 10.1021/acs.energyfuels.5b00905
Energy Fuels XXXX, XXX, XXX−XXX

DISCUSSION

While MgO has not been reported as an additive for liquid propellants, many researchers have shown that the addition of other nanoparticles to liquid fuels improve their evaporation rates due to contributing factors, such as exposed surface area and concentration.[3,26−28] Additionally, particulate additives have been shown to improve heat transfer in the droplet and enhance evaporation.[8]

The contribution of MgO to regression behavior is shown in Figure 3 with the addition of a third stage identified by an inflection point in the slope of the droplet diameter as a function of time. RP-2 boils at 176 °C, while the dispersant boils at 360 °C.[29] For this reason, RP-2 combustion likely precedes that of the dispersant. Also, Javed et al.[3] showed that the addition of OA-coated Al particles to kerosene resulted in a third stage of evaporation, similar to observations here. Javed et al.[3] associated the third stage with combustion of the dispersant that vaporizes at a higher temperature than the liquid fuel, also consistent with results shown here.

As shown in Table 3, adding MgO introduces a heating period (stage 1), stage 2 is reduced significantly, and stage 3 is introduced associated with OA combustion. Tables 3 and 4 clearly indicate that MgO accelerates regression via reduced times and increases the droplet surface regression rate during stage 2. The droplet regression rate may increase with an increased number of nucleation sites available as a result of the presence of well-dispersed MgO. Panels B and C of Figure 4 are still frame images of RP-2 with 0.25 wt % MgO during stage 2 and clearly show several localized combustion sites, illustrating disruptive burning induced by the solid particles. The image shows ripples in the droplet surface akin to nucleation sites, indicating the presence of MgO particles. Panels B and C of Figure 4 also indicate a uniform distribution of nucleation sites, indicating that MgO particles at 0.25 wt % concentration may not agglomerate significantly. Negligible disruptive burning is observed in RP-2 samples without an additive (Figure 4A).

However, there is an upper limit on the MgO concentration that will improve regression. Burn rate constants shown in Table 3 indicate that the effect of the particle concentration on regression rate is linked to stages 2 and 3. Below 0.5 wt % MgO, there are not enough particles to promote stage 3 combustion. In other words, droplet regression is hindered by reduced combustion in stage 3, associated with combustion of the stabilizer. It may be that particles are consumed or escape in the gas phase products during stage 2 such that the lack of particles in stage 3 hinders heat transfer. It is also noted that a residue left on the fiber for even the smallest MgO concentrations varied as a function of the MgO concentration and accounts for the normalized graphs shown in Figure 3 not going to zero. Figure S3 shows the residue concentration remaining on the fiber as a function of the MgO concentration. As the particle concentration increases, the residue remaining on the fibers decreases, as shown in Figure S3. If particle agglomeration increases with the particle concentration but the residue decreases, then either particles may become entrapped in the gas-phase products and removed from the droplet during stage 2, resulting in less residue being deposited on the fiber, the oxide particles react with hydrocarbons to form carbon oxides and Mg or MgO as nanoparticles, or nanoparticle agglomerates may escape within the gaseous products of combustion. Also, K_b is highest for stage 3 for 0.75 wt % MgO, but at this high concentration, particle agglomeration may begin to hinder regression during stage 2 because, at 0.75 wt % MgO stage 2, K_b is reduced 85% from the 0.50 wt % MgO stage 2 case. If agglomeration is responsible for the decreasing trend in stage 2 with increasing the MgO concentration, then one would expect greater residue remaining on the fiber, when in fact less is observed. Therefore, the reduced regression behavior observed for 1 wt % MgO may result from agglomerations that escape the droplet via gas-phase combustion products and, thereby, hinder regression. In this way, a balance is needed to have enough particles to optimize heat transfer during both stages 2 and 3 but not introduce agglomeration. At 0.5 wt % MgO, K_b for stages 2 and 3 are optimized and a balance is achieved.

Interestingly, a similar trend observed in Tables 3 and 4 with regression rate and burn rate constant was observed by Javed et al.[3] on evaporation rate with Al particles. Specifically, Javed et al.[3] observed a maximum evaporation rate at 0.50 wt % Al suspension in an 800 °C environment, and a maximum regression rate at 0.50 wt % MgO was also observed here. However, the burn rate constants observed here are as high as 111.8 mm^2/s, while the evaporation rate constants reported by Javed et al.[3] are as high as 1.1 mm^2/s. The following analysis shows that MgO particles provide competitive thermal diffusive heat transfer to Al but superior radiant heat transfer, and it is radiation that may be promoting the high burn rate constants and regression rates observed. As a comparison between the diffusive and radiant heat transfer mechanisms, the thermal properties listed in Table 1 for Al and MgO can be used to quantify relevant time scales. The thermal diffusion time scale is estimated as $\tau_{diff} = L^2/\alpha$, where L is a characteristic length (i.e., particle diameter) and α is the thermal diffusivity (see Table 1). For Al (70 nm as in Javed et al.,[3]) τ_{diff} is 0.056 ns, and for MgO (20 nm), τ_{diff} is 0.029 ns. The radiant time scale is calculated as $\tau_{rad} = \rho V C_p/hA$, where ρ is the density, V is the particle volume, C_p is the heat capacity, h is the radiation heat transfer coefficient, and A is the surface area of the particle.[30] The radiation heat transfer coefficient, h, is calculated from $h = \varepsilon\sigma(T_s + T_\infty)(T_s^2 + T_\infty^2)$.[30] In this equation, σ is the Stefan−Boltzmann constant, 5.67×10^{-8} W m^{-2} K^{-4},[30] ε is the emissivity of the nanoparticle (given in Table 1), and T_s and T_∞ are the RP-2 boiling and ambient temperatures, respectively. For Al (70 nm from Javed et al.[3]), τ_{rad} is 18.2 ms, but for MgO, τ_{rad} is 1.54 ms. Interestingly, MgO is of the same order as Al for the diffusion time scale but an order of magnitude faster than Al for the thermal radiation time scale. Similarly, assuming 20 nm Al, τ_{diff} is 0.0046 ns and τ_{rad} is 5.2 ms. These calculations are summarized in Table 5.

These calculations show that particle size influences may be even more significant than thermophysical properties at controlling diffusion and radiant time scales for enhancing heat transfer in nanofluids. The diffusive time scale is on the order of nanoseconds, while the radiation time scale is on

Table 5. Summary of Radiation and Diffusion Time Scale Calculations[a]

material	characteristic time (conduction/diffusion) (ns)	characteristic time (radiation) (ms)
MgO (20 nm)	0.0299	1.54
Al (70 nm)	0.0558	18.2
Al (20 nm)	0.0045	5.2

[a]Particle size is indicated in parentheses next to the material.

DOI: 10.1021/acs.energyfuels.5b00905
Energy Fuels XXXX, XXX, XXX−XXX

milliseconds order. This ultimate increase in diffusive behavior promoted by particle size decrease is responsible for enhanced and rapid heating. From this analysis, MgO optimization of regression and burn rate constant may be attributed to enhanced conductive/diffusive energy transport, owing to particle size, and is optimized by the solid particle concentration according to balanced burn rate constants during stages 2 and 3 of regression.

CONCLUSION

Liquid propellant RP-2 with MgO nanoparticle additives that are coated with OA to improve their dispersion properties was shown to produce up to 2 orders of magnitude higher regression rates compared to pure RP-2. Measured surface tension and calorific output have a negligible effect on combustion enhancements. Instead, the mechanism controlling enhanced combustion is heat transfer, and specifically, diffusive thermal time scales are on the order of 0.03 ns and controlled largely by the particle size. The MgO particles promote nucleation and disruptive burning of RP-2. There is an optimum MgO threshold concentration of 0.5 wt % MgO that balances the stages of regression. Below this threshold, MgO particles poorly promote combustion of the dispersant, and that hinders overall regression. Beyond this threshold, MgO particles may lead to agglomeration. Overall, this study reveals that the key to optimizing RP-2 combustion is by introducing a specific concentration of well-dispersed nanoparticles that purposefully enhances conductive heat transfer. This understanding has fundamental implications for many liquid fuels and nanofluids in general.

ASSOCIATED CONTENT

Supporting Information

The Supporting Information is available free of charge on the ACS Publications website at DOI: 10.1021/acs.energyfuels.5b00905.

Curve fits for stages of regression of RP-2 with 0.25 wt % MgO, RP-2 with 0.50 wt % MgO, RP-2 with 0.75 wt % MgO, and RP-2 with 1.0 wt % MgO (Figure S1), droplet diameter squared histories of RP-2 containing various concentrations of MgO: pure RP-2, with 0.050 wt % MgO, with 0.25 wt % MgO, with 0.50 wt % MgO, with 0.75 wt % MgO, and with 1.0 wt % MgO (Figure S2), residue on quartz fiber for various MgO concentrations (Figure S3), and still frame images showing residue on quartz fiber for 1.0 and 0.5 wt % MgO concentrations (Figure S4) (PDF)

AUTHOR INFORMATION

Corresponding Author

*Telephone: 806-834-3733. E-mail: michelle.pantoya@ttu.edu.

Notes

The authors declare no competing financial interest.

ACKNOWLEDGMENTS

The authors are grateful for support from the Air Force Office of Scientific Research (AFOSR) Contract FA9300-13-M-1006 and encouragement from their program manager, Dr. Alex Schumaker. Michelle L. Pantoya, Michael N. Bello, and Keerti Kappagantula are grateful for support from the Army Research Office Contracts W911NF-11-1-0439 and W911NF-14-0250 and encouragement from their program manager, Dr. Ralph Anthenien.

REFERENCES

(1) Sutton, G. P.; Biblarz, O. *Rocket Propulsion Elements*, 8th ed.; John Wiley and Sons: Hoboken, NJ, 2010.

(2) Javed, I.; Baek, S. W.; Waheed, K. Effects of dense concentrations of aluminum nanoparticles on the evaporation behavior of kerosene droplet at elevated temperatures: The phenomenon of microexplosion. *Exp. Therm. Fluid Sci.* **2014**, *56*, 33−44.

(3) Javed, I.; Baek, S. W.; Waheed, K.; Ali, G.; Cho, S. O. Evaporation characteristics of kerosene droplets with dilute concentrations of ligand-protected aluminum nanoparticles at elevated temperatures. *Combust. Flame* **2013**, *160* (12), 2955−2963.

(4) Gan, Y.; Qiao, L. Combustion characteristics of fuel droplets with addition of nano and micron-sized aluminum particles. *Combust. Flame* **2011**, *158* (2), 354−368.

(5) Roy Choudhury, P. Slurry fuels. *Prog. Energy Combust. Sci.* **1992**, *18* (5), 409−427.

(6) Gan, Y. Combustion and evaporation characteristics of fuel droplets containing suspended energetic nanoparticles. Ph.D. Thesis, Purdue University, West Lafayette, IN, 2012; p 162.

(7) Pivkina, A.; Ulyanova, P.; Frolov, Y.; Zavyalov, S.; Schoonman, J. Nanomaterials for Heterogeneous Combustion. *Propellants, Explos., Pyrotech.* **2004**, *29* (1), 39−48.

(8) Gan, Y.; Qiao, L. Optical properties and radiation-enhanced evaporation of nanofluid fuels containing carbon-based nanostructures. *Energy Fuels* **2012**, *26* (7), 4224−4230.

(9) Wang, X.; Xu, X.; Choi, S. U. S. Thermal Conductivity of Nanoparticle - Fluid Mixture. *J. Thermophys. Heat Transfer* **1999**, *13* (4), 474−480.

(10) Chen, R. H.; Phuoc, T. X.; Martello, D. . Surface tension of evaporating nanofluid droplets. *Int. J. Heat Mass Transfer* **2011**, *54* (11−12), 2459−2466.

(11) Tyagi, H.; Phelan, P. E.; Prasher, R.; Peck, R.; Lee, T.; Pacheco, J. R.; Arentzen, P. Increased hot-plate ignition probability for nanoparticle-laden diesel fuel. *Nano Lett.* **2008**, *8* (5), 1410−1416.

(12) Allen, C.; Mittal, G.; Sung, C. J.; Toulson, E.; Lee, T. An aerosol rapid compression machine for studying energetic-nanoparticle-enhanced combustion of liquid fuels. *Proc. Combust. Inst.* **2011**, *33* (2), 3367−3374.

(13) Van Devener, B.; Anderson, S. L. Breakdown and combustion of JP-10 fuel catalyzed by nanoparticulate CeO_2 and Fe_2O_3. *Energy Fuels* **2006**, *20* (5), 1886−1894.

(14) Javed, I.; Baek, S. W.; Waheed, K. Evaporation characteristics of heptane droplets with the addition of aluminum nanoparticles at elevated temperatures. *Combust. Flame* **2013**, *160* (1), 170−183.

(15) *CRC Handbook of Chemistry and Physics*; Haynes, W. M., Ed.; CRC Press: Boca Raton, FL, 2014.

(16) ASM International Materials Properties Database Committee. *ASM Ready Reference: Thermal Properties of Metals*; ASM International: Materials Park, OH, 2002.

(17) Pradyot, P.*Handbook of Inorganic Chemicals*; McGraw-Hill: New York, 2002.

(18) Helmboldt, O.; Hudson, L. K.; Misra C.; Wefers, K.; Heck, W.; Stark, H.; Rösch, N. Aluminum compounds, inorganic. *Ullmann's Encyclopedia of Industrial Chemistry*; Wiley-VCH: Weinheim, Germany, 2007.

(19) Shand, M. A. *The Chemistry and Technology of Magnesia*; John Wiley and Sons: Hoboken, NJ, 2006.

(20) Datta, S.; Dikici, B.; Pantoya, M. L.; Ekwaro-Osire, S. Reaction Dynamics and Probability Study of Aluminum-Viton-Acetone Droplets. *J. Propul. Power* **2011**, *27* (2), 396−401.

(21) Struk, P. M.; Ackerman, M.; Nayagam, V.; Dietrich, D. L. On calculating burning rates during fiber supported droplet combustion. *Microgravity Sci. Technol.* **1998**, *11*, 144−151.

(22) ASTM International. *ASTM Standard D240.09, Standard Test Method for Heat of Combustion of Liquid Hydrocarbon Fuels by Bomb Calorimeter*; ASTM International: West Conshohocken, PA, 2009.

DOI: 10.1021/acs.energyfuels.5b00905
Energy Fuels XXXX, XXX, XXX−XXX

(23) Tucker, W. B. Surface tension by pendant drops. Sc.D. Thesis, Massachusetts Institute of Technology (MIT), Cambridge, MA, 1938; p 147.
(24) Stauffer, C. E. The Measurement of Surface Tension by the Pendant Drop Technique. *J. Phys. Chem.* **1965**, *69* (6), 1933−1938.
(25) Turns, S. R. *An Introduction to Combustion: Concepts and Applications*, 2nd ed.; McGraw-Hill: New York, 2000.
(26) Chen, R. H.; Phuoc, T. X.; Martello, D. Effects of nanoparticles on nanofluid droplet evaporation. *Int. J. Heat Mass Transfer* **2010**, *53* (19−20), 3677−3682.
(27) Gan, Y.; Qiao, L. Evaporation characteristics of fuel droplets with the addition of nanoparticles under natural and forced convections. *Int. J. Heat Mass Transfer* **2011**, *54* (23−24), 4913−4922.
(28) Gan, Y.; Qiao, L. Radiation-enhanced evaporation of ethanol fuel containing suspended metal nanoparticles. *Int. J. Heat Mass Transfer* **2012**, *55* (21−22), 5777−5782.
(29) Alfa Aesar. Research Chemicals, Metals and Materials. A Johnson Matthey Company.
(30) Incropera, F. P.; Dewitt, D. P. *Fundamentals of Heat and Mass Transfer*, 5th ed.; John Wiley and Sons: Hoboken, NJ, 2002.
(31) Irvin, D. Personnel commnication. Systems and Materials Research Corporation, Austin, TX, 2014.
(32) Law, C. K. Recent advances in droplet vaporization and combustion. *Prog. Energy Combust. Sci.* **1982**, *8*, 171−201.

DOI: 10.1021/acs.energyfuels.5b00905
Energy Fuels XXXX, XXX, XXX−XXX